Experimental and theoretical study of skylight polarization transmitted through Snell's window of a flat water surface

Shai Sabbah

The Interuniversity Institute of Eilat, P.O. Box 469, 88103 Eilat, Israel, and Evolution, Systematics, and Ecology (ESE) Department, Life Sciences Institute, The Hebrew University, Jerusalem 91904, Israel

András Barta, József Gál, and Gábor Horváth

Bio-optics Laboratory, Department of Biological Physics, Loránd Eötvös University, H-117 Budapest, Hungary

Nadav Shashar

The H. Steinitz Marine Biology Laboratory, P.O. Box 469, 88103 Eilat, Israel, and Evolution, Systematics, and Ecology (ESE) Department, Life Sciences Institute, The Hebrew University, Jerusalem 91904, Israel

Received May 18, 2005; revised December 11, 2005; accepted March 10, 2006; posted March 16, 2006 (Doc. ID 62216)

The celestial polarization pattern may be scrambled by refraction at the air–water interface. This polarization pattern was examined in shallow waters with a submersible polarimeter, and it was calculated by using land measurements ("semiempirical predictions") and models of the skylight polarization. Semiempirically predicted and measured *e*-vector orientations were significantly similar. Conversely, predicted percent polarization was correlated but lower than measurements. Percent polarization depended on wavelength, where at high sun altitudes maximal percent polarization generally appeared in the UV and red spectral regions. The wavelength dependency of polarization may lead to differential spectral sensitivity in polarization-sensitive animals according to time and type of activity. © 2006 Optical Society of America

OCIS codes: 260.5430, 120.5410, 170.1420.

1. INTRODUCTION

Snell's window is the circular region on the water surface above an underwater observer with an aperture angle of approximately 97.5°, within which the entire celestial hemisphere above the water is compressed due to refraction. This area is often seen as a bright circle at the water surface by submerged observers.[1] The underwater light field is partially linearly polarized,[2,3] except for some elliptical polarization near the water surface.[4] In shallow waters, the linear polarization pattern has been divided into two parts, one inside Snell's window and the other outside it.[5]

Generally, the polarization pattern within Snell's window near the water surface and a few meters deep is assumed to be determined by the same factors as those influencing the skylight polarization. Therefore sun position, cloud cover, amount of atmospheric dust and haze, distance of the direction of observation from the zenith, and multiple scattering all affect the polarization pattern within Snell's window.[5] Marine animals use this refracted celestial polarization pattern, which is highly correlated with the sun position, for navigational tasks.[6]

Using the Fresnel theory of refraction and the single-scattering Rayleigh model of skylight polarization, Horváth and Varjú[7] computed the influence of refraction on the celestial polarization patterns visible within Snell's window of the flat water surface for four sun altitudes. These calculations were limited in that they assumed a totally flat water surface (no surface waves) and single-scattering Rayleigh skylight from a totally clear sky. However, due to the focusing of sunlight by surface waves[8–10] and the wavelength-dependent attenuation of light in water,[11] deviations from this model are likely to occur. Indeed, Cronin and Shashar,[12] measuring polarization at 15 m deep on a coral reef, did not find substantial differences between the polarization patterns within and outside Snell's window in the 350–600 nm spectral range. Additionally, neither polarization measurements conducted in artificial turbid media[13] nor measurements performed at sea and in freshwater lakes[14,15] reported differences between the two proposed patterns.

Polarization-sensitive animals utilize the underwater polarization patterns in various manners.[2,6,16] Notable in the current context are body orientation and navigation.[17–25] Use of a polarization-based sun compass is well-known in fishes swimming close to the water surface.[26] In calm shallow waters, the apparent location of the sun can be readily observed within Snell's window. However, with the general undulating water surface and with increasing depth, the determination of the sun position becomes difficult.[27] Since skylight polarization transmitted through Snell's window depends on the sun

1084-7529/06/081978-11/$15.00

position,[5] utilizing this polarization pattern for orientation and navigation may confer an indirect sun compass. Hence, in terrestrial as well as marine animals, the distribution of polarization of skylight is important in orientation and navigation tasks.[16] Hawryshyn and McFarland[28] as well as Parkyn and Hawryshyn[29] suggested that fishes make use of the UV component of the polarization pattern, which is abundant inside Snell's window[30] for body orientation and navigation. As another mode of navigation, the grass shrimp (*Palaemonetes vulgaris*) exploits the polarization pattern of Snell's window in its offshore escape response.[31–34]

Another means by which marine animals may utilize the skylight polarization transmitted through Snell's window is to enhance the apparent contrast of objects.[16] The polarization of light that scatters from a transparent object, e.g., zooplankton,[35] or that is reflected off a light-reflecting silvery fish[36,37] differs from that of the incident skylight. Thus a polarization-sensitive animal could perceive these differences and detect the otherwise camouflaged predator or prey.

As a consequence of the above, revealing the way the celestial polarization pattern changes as it penetrates into the water is central for understanding the visual input available to polarization-sensitive marine animals and its potential use.

In this study, we (i) performed a quantitative comparison between theoretical predictions and *in situ* measurements of the polarization of skylight transmitted through Snell's window, (ii) examined the spectral distribution of this polarization, and (iii) drew predictions regarding the polarization information available to animals and the potential adaptations of animals for utilizing this information.

2. MATERIALS AND METHODS

A. Underwater Polarization Measurements

Examination of the spatiotemporal and spectral characteristics of the underwater polarization pattern within Snell's window was conducted (by S. Sabbah and N. Shashar) over a coral reef in front of the H. Steinitz Marine Biology Laboratory, Eilat, Red Sea (29°30′ N, 34°56′ E).

Recordings were performed by using a custom-built rapid-sampling point-source polarimeter described in detail by Shashar *et al.*[11] The polarimeter was based on a three-channel spectrophotometer (Ocean Optics ADC-1000-USB), each channel equipped with a fiber optic (Ocean Optics UV/VIS 600 μm) with a 5° acceptance angle restrictor, a polarization-neutral, spectrum-flattening, color filter (Rosco Supergel #02, bastard amber), and a linear polarizer (Polaroid HNP′B UV/VIS). The transmission axes of the polarizers were set to 0°, 45°, and 90° off the horizon. The three fibers' heads and filters were inserted into a submersible housing that was fixed on a rotating apparatus, attached to a vertical pole at a depth of 2 m. Integration times ranged between 1 and 5000 ms to allow a sufficient signal-to-noise ratio within the 350–700 nm spectral range. To surmount wave-induced fluctuations in the readings, we applied automatic averaging of several integrated recordings to provide a total recording duration of no less than 3 s per measurement, which was much higher than the waves' undulation period.

Measurements were completed in August 2003 under clear blue skies. The detector was aligned at an elevation of 60° above the horizon, and each morning the detector was adjusted to face one of five relative directions D_n ($n=1,2,\ldots,5$) corresponding to 0°, 45°, 90°, 135°, and 180° away from the solar meridian at sunrise, and stayed fixed throughout the day. A measurement day commenced at a sun altitude of −5° and continued until midday, when the sun reached its highest altitude. Eilat, at the tip of the Gulf of Aqaba, is surrounded by the Edom and Eilat mountains. At sunrise the sun was obscured by mountains until it reached an elevation of 2°–3°. Therefore solar azimuth at sunrise was defined as the azimuth at which the sun peeked over the mountains.

Measurements were taken every minute continuously. Each measurement was coupled with the corresponding sun altitude and the horizontal azimuth angle (measured at a 1° resolution) between the sun and the detector's direction (Fig. 1). Data on the sun position were obtained from a U.S. Navy website (http://aa.usno.navy.mil/data/

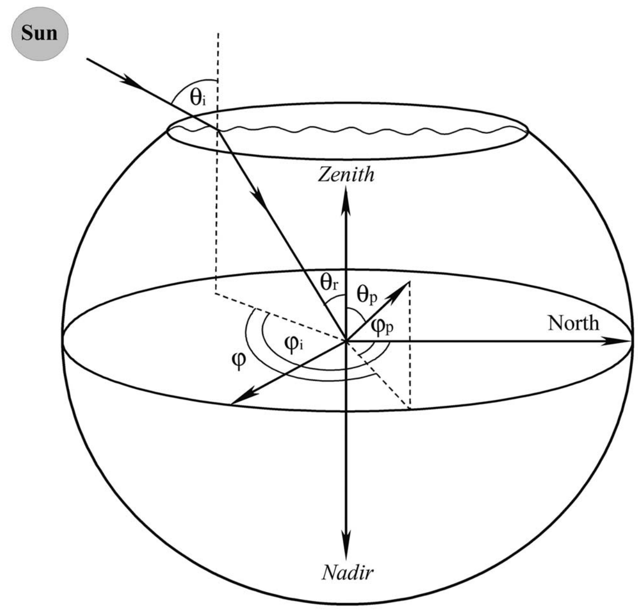

Fig. 1. Definition of light directionality and measurements in the underwater setup. The solar zenith angle (θ_i)—the vertical angle between the zenith and the sun as viewed from outside the water—ranges from 0°, when the sun is at the zenith, to 90°, when the sun is at the horizon, to angles greater than 90°, when the sun is below the horizon; the vertical angle between the refracted light beam and the zenith (θ_r) ranges from 0°, when the sun is at the zenith, to 48.6°, when the sun is at the horizon, to larger angles, when the sun is below the horizon; the detector zenith angle (θ_p; also referred to as the viewing zenith angle)—the vertical angle between the zenith and the detector—ranges from 0°, when the detector is facing the zenith, to 90°, when the detector is facing horizontally, to 180°, when the detector is pointing toward the nadir; the solar and detector azimuth angles φ_i and φ_p are the horizontal angles between the north direction and the sun or the detector, respectively (the azimuth angles are measured clockwise from the north when looking downward); and the relative direction (φ) is the horizontal angle between the two vertical planes containing the sun and the detector.

docs/AltAz.html). Throughout this project, over 1000 polarization measurements were executed and analyzed.

B. Data Processing and Analysis of Underwater Measurements

Before measurement setup, fibers were cross calibrated by examining an evenly illuminated white diffusing fabric. By accounting for the cross calibration factors and dark noise measurements, we calculated the intensity I, percent polarization d, and e-vector orientation α of light by using a custom-made LabView application. Polarization analysis was based on the equations of Wolff and Andreou,[38] modified by Shashar *et al.*[11] In short, if I_0, I_{45}, and I_{90} represent the intensity values recorded when the polarizing filter on a fiber optic is at 0°, 45°, and 90° from the instrument horizon, respectively, then, from geometrical considerations, the orientation of polarization θ (representing the e-vector shift from the vertical) is given by

$$\theta = \left(\frac{1}{2}\right)\arctan\left(\frac{I_0 + I_{90} - 2I_{45}}{I_{90} - I_0}\right),$$

$$\text{Then if } (I_{90} < I_0)\ [\text{if } (I_{45} < I_0)\ \theta = \theta + 90°\ \text{ else } \theta = \theta - 90°]. \tag{1}$$

And if a switch is made from a shift off the vertical scale to one off a horizontal scale, i.e., absolute e-vector orientation α, the following condition is applied:

$$\text{if } (\theta > 90°)\ \alpha = \theta - 90°\ \text{ else } \alpha = \theta + 90°. \tag{2}$$

The total intensity is given by

$$I = I_0 + I_{90}, \tag{3}$$

while the percent polarization is given by

$$d = 100\frac{\sqrt{(I_0 - I_{90})^2 + (2I_{45} - I_{90} - I_0)^2}}{I_0 + I_{90}}. \tag{4}$$

The e-vector orientation scale ranges between 0° and 180°, with 0° and 180° corresponding to horizontal polarization and 90° corresponding to a vertical e-vector, and the percent polarization ranges between 0% and 100%.

C. Measurement Controls and Limitations

Several levels of controls were executed. (i) Performing intensity-controlled polarization measurements, one found the minimal intensity level at which a reliable polarization measurement could be obtained. The latter intensity level plus its square root (approximation of the noise level) was defined as the minimum level of signal usable for analysis. Measurements lower than this minimal level were excluded from analysis. (ii) Due to the local tide, the detector depth changed by up to 1 m during each measuring day. In a control experiment, examining the effect of this change on the underwater polarization, maximal standard deviations of 4.32% and 4.68° for d and α, respectively, were found. (iii) Variation between days was established by performing a series of 30 measurements, 1 min apart, on each of three days, with the detector facing an elevation of 60° above the horizon. On these days, recordings were performed at similar sun altitudes and horizontal azimuth angles between the sun and the detector's direction, yielding 30 triplets in which the sun altitude and the relative direction off the solar azimuth were nearly identical (less than 1° difference). Within the 350–700 nm spectral range and at individual wavelengths spaced with a 10 nm interval, the standard deviation (SD) between the members of each triplet was calculated. Throughout the examined spectrum, the SDs of the 30 triplets did not exceed 5° and 5% for α and d, respectively. Thus measurements taken on different days were comparable.

D. Full-Sky Polarization Measurements

The full-sky polarimetric measurements have been performed by a different but overlapping group of authors in 1999 in Tunisia.[39] The full-sky polarimeter and the evaluation procedure were described in detail by Gál *et al.*[40] Here we mention only the following technical data: In our case, a 180° field of view was obtained (under clear skies over an open desert, by A. Barta, J. Gál, and G. Horváth) by using a fisheye lens (Nikon Nikkor, f=2.8, focal length 8 mm) with a built-in rotating disk mounted with three broadband (275–750 nm) neutral density, linearly polarizing filters (Polaroid HNP′B) having three polarization axes (0°, 45°, and 90° from the radius of the disk). The detector was a photo emulsion (Fujichrome Sensia II 100 ASA color reversal film; the maxima and half-bandwidths of its spectral sensitivity curves were $\lambda_{red}=650\pm30$ nm, $\lambda_{green}=550\pm30$ nm, and $\lambda_{blue}=450\pm50$ nm) in a roll-film photographic camera (Nikon F801). For a given sky, three photographs were taken for the three alignments of the transmission axis of the polarizers. The camera was set on a tripod such that the optical axis of the fisheye lens was vertical. Using a personal computer, after evaluation of the three chemically developed color pictures for a given sky and 24-bit (3×8 for red, green, and blue) digitization (using a Hewlett Packard ScanJet 6100C), the patterns of intensity I, percent polarization d, and e-vector orientation α of skylight were determined as high-resolution, color-coded, two-dimensional circular maps. These patterns were obtained in the red, green, and blue spectral ranges, in which the three color-sensitive layers of the photo emulsion used have maximal sensitivity. However, one should note that in this full-sky image we do not have exact spectral information.

E. Calculation of the Percent Polarization and *e*-Vector Orientation of Linear Polarization of Skylight Transmitted through Snell's Window of a Flat Water Surface

The boundary of Snell's window of a flat water surface extends up to

$$\beta_{SW} = \arcsin\left(\frac{1}{n}\right) = \arcsin\left(\frac{1}{1.33}\right) = 48.75° \tag{5}$$

measured from the zenith, where $n=1.33$ is the refractive index of water. Due to refraction of light at the air–water interface, the world above the water visible through Snell's window is distorted.[41] A point of the firmament with an elevation angle β measured from the horizon is apparently seen with an elevation angle

$$\beta^* = \arccos\left(\frac{\cos\beta}{n}\right). \quad (6)$$

The apparent horizon corresponds to the boundary of Snell's window. Due to refraction, the state of polarization of skylight transmitted through the water surface also changes. To describe the state of polarization of skylight, we used the additive Stokes vector[16]:

$$\mathbf{S} = (I,Q,U,V), \quad (7)$$

where the first component I is the total intensity of light. The second component

$$Q = Id\cos(2\alpha)\cos(2\epsilon) \quad (8)$$

quantifies the fraction of linear polarization parallel to a reference plane, where d is the percent polarization, α is the e-vector orientation, and ε is the ellipticity of polarization. The third component

$$U = Id\sin(2\alpha)\cos(2\epsilon) \quad (9)$$

gives the proportion of linear polarization at 45° with respect to the reference plane, and the fourth component

$$V = Id\sin(2\epsilon) \quad (10)$$

describes the fraction of right-handed circular polarization. Since the circular polarization of skylight is practically zero,[16] we used $\epsilon=0$ [when $\cos(2\epsilon)=1$, $\sin(2\epsilon)=0$, and $V=0$] in this work. The change in the state of polarization of skylight refracted at the air–water interface and transmitted through Snell's window of a flat water surface can be described by the following Mueller matrix[41]:

$$\mathbf{M} = \frac{\sin(2\theta_i)/\sin(2\theta_r)}{2\sin^2(\theta_i+\theta_r)/\cos^2(\theta_i-\theta_r)} \times \begin{bmatrix} \cos^2(\theta_i-\theta_r)+1 & \cos^2(\theta_i-\theta_r)-1 & 0 & 0 \\ \cos^2(\theta_i-\theta_r)-1 & \cos^2(\theta_i-\theta_r)+1 & 0 & 0 \\ 0 & 0 & 2\cos(\theta_i-\theta_r) & 0 \\ 0 & 0 & 0 & 2\cos(\theta_i-\theta_r) \end{bmatrix}, \quad (11)$$

where θ_i and θ_r are the angles of incidence and refraction measured from the vertical, respectively. The elements of this Mueller matrix originate in the Fresnel theory of polarization of light transmitted through the air–water interface. If the Stokes vectors of the incident and transmitted (i.e., refracted) skylight are $\mathbf{S}_i$ and $\mathbf{S}_t$, then

$$\mathbf{S}_t = \mathbf{M}\cdot\mathbf{S}_i. \quad (12)$$

In the semiempirical prediction, we used the patterns of the intensity I, percent polarization d, and e-vector orientation α of partially linearly polarized light arriving from clear skies as presented earlier by Pomozi *et al.*[39] These patterns were measured by full-sky imaging polarimetry in Tunisia at wavelengths 650 nm (red), 550 nm (green), and 450 nm (blue). The sun altitudes θ_S for the measured celestial patterns are approximately ±0.5°, the same as those for the underwater measurements. The azimuth angles φ of the underwater measurements were transformed to ensure that they coincide with those of the celestial measurements.

The I, d, and α patterns of the Rayleigh sky at a given sun position were calculated on the basis of the single-scattering Rayleigh theory.[42] In the single-scattering Rayleigh atmosphere, the intensity $I_{\text{Rayleigh}}(\gamma)$ and percent polarization $d_{\text{Rayleigh}}(\gamma)$ of skylight are

$$I_{\text{Rayleigh}}(\gamma) = \frac{I_{\max}}{2}(1+\cos^2\gamma), \quad (13)$$

$$d_{\text{Rayleigh}}(\gamma) = d_{\max}\frac{1-\cos^2\gamma}{1+\cos^2\gamma}, \quad (14)$$

independent of the wavelength, where γ is the angular distance between the sun and the point investigated. The value of $I_{\max}$ was chosen arbitrarily, because all the Stokes parameters given in Eqs. (7)–(10) are proportional to I, and thus d [see Eq. (15)] and α [see Eq. (16)] are independent of $I_{\max}$. The value of $d_{\max}$ was chosen as the maximal d value in the celestial d pattern measured in the green (550 nm). In the single-scattering Rayleigh atmosphere, the e-vector direction of skylight is perpendicular to the plane of scattering determined by the observer, the point observed, and the sun, independent of the wavelength.

To be compatible with the underwater as well as the aerial sky polarization measurements, we calculated the d and α patterns of the transmitted skylight in Snell's window. If $V=0$, d and α can be expressed by the Stokes parameters as follows[16]:

$$d = \frac{\sqrt{Q^2+U^2}}{I}, \quad (15)$$

$$\alpha = \frac{1}{2}\arctan\left(\frac{U}{Q}\right). \quad (16)$$

The full-sky I, d, and α patterns of clear skies originated from two sources: (i) the I, d, and α patterns measured earlier by Pomozi *et al.*[39] at 650, 550, and 450 nm and (ii) the I, d, and α patterns calculated from the single-scattering Rayleigh theory. The I, d, and α patterns of the transmitted skylight are called "semiempirical" or "Rayleigh" if the celestial I, d, and α patterns originate from source (i) or (ii), respectively.

As noted in Subsection 2.A, the underwater polarization measurements (Fig. 1) were performed in five directions of view D_n ($n=1,2,\ldots,5$). To compare the measured and predicted d and α values of skylight transmitted through Snell's window, we calculated d and α at D_n in the following way: At every D_n, first the Stokes parameters I, Q, and U were calculated from the semiempirical or Rayleigh I, d, and α values of each point in the 10° field of view of the underwater polarimeter with the use of Eqs. (7)–(9). Then the individual Stokes vectors were summed up in the field of view, resulting in the predicted Stokes vector.[43] Finally, using Eqs. (15) and (16), in calculated the predicted d and α values from the predicted Stokes vector.

F. Statistics

Due to the nonnormal distribution of the data, nonparametric statistics were used. All statistical analyses were performed with STATISTICA software. The degree of fit between the semiempirical calculations and the measured percent polarization was defined as $d_{\text{semiempirical}} - d_{\text{measured}}$, while the degree of fit between the theoretical prediction and the measured percent polarization was defined as $d_{\text{Rayleigh}} - d_{\text{measured}}$. Similarly, the degree of fit was also calculated for the e- vector orientation α. Using the nonparametric ANOVA, Kruskal–Wallis test, we examined the effects of the sun altitude and the light hue on the various degrees of fit. To compare the pooled polarization values within Snell's window (through all examined sun altitudes and directions) calculated by using the celestial Rayleigh pattern (d_{Rayleigh} and α_{Rayleigh}) versus those calculated by using the measured celestial pattern ($d_{\text{semiempirical}}$ and $\alpha_{\text{semiempirical}}$), we applied the nonparametric Wilcoxon test. Similar analyses were also used to compare the pooled polarization values within Snell's window, measured and predicted either by the semiempirical calculations ($d_{\text{semiempirical}}$ and $\alpha_{\text{semiempirical}}$) or by the celestial Rayleigh pattern (d_{Rayleigh} and α_{Rayleigh}). To characterize the precise relationship between the measured polarization values and the theoretical or semiempirical predictions, we used the nonparametric sign test and linear regression. Throughout this manuscript n = number of replicates or measurements, and p = level of confidence.

3. RESULTS

The skylight polarization pattern transmitted through Snell's window, calculated by using either the measured or the Rayleigh celestial patterns, could describe the general pattern of polarization, as measured from under water, in both e-vector orientation α and percent polarization d (Figs. 1 and 2). Within Snell's window, the measured d and the absolute tilt of the e-vector orientation $|\alpha|$ ranged between 0% and 73% and 0° and 90°, respectively. The degree of fit between the semiempirical calculations and the

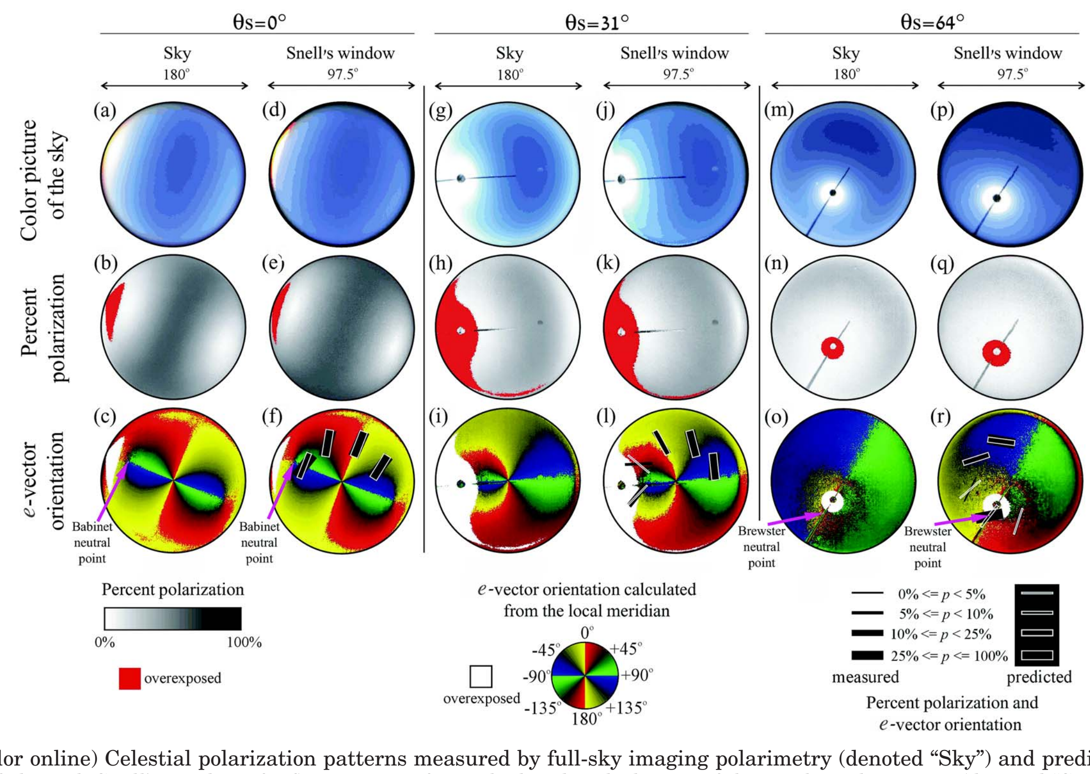

Fig. 2. (Color online) Celestial polarization patterns measured by full-sky imaging polarimetry (denoted "Sky") and predicted sky patterns viewed through Snell's window of a flat water surface calculated with the use of these celestial patterns (denoted "Snell's window") at sun altitudes $\theta_S = 0°$, 31°, and 64°. The center and the perimeter of the celestial patterns are the zenith and the horizon, respectively, while, in Snell's window, the center and the perimeter of patterns due to refraction of light represent the zenith and Snell's window boundary, respectively. (a), (g), (m) 180° field-of-view color photographs of the clear sky; (d), (j), and (p) 97.5° field-of-view color pictures of the sky visible through Snell's window. For each sun altitude, the celestial and Snell's window patterns of the percent polarization d and e-vector orientation α (measured clockwise from the local meridian) in the green (550 nm) region of the spectrum are presented. In the measured d and α patterns, the overexposed celestial regions are shaded by red and white, respectively, and the radial black bar in the measured patterns is the wire of the sun occulter (a small black disk). In the α patterns, black bars and white rectangles represent the measured and predicted d and α at four detector positions (coinciding with the centers of the bars). The alignment of the bars and rectangles shows the orientation of polarization, while their width corresponds to four ranges of d, shown in the inset at the bottom.

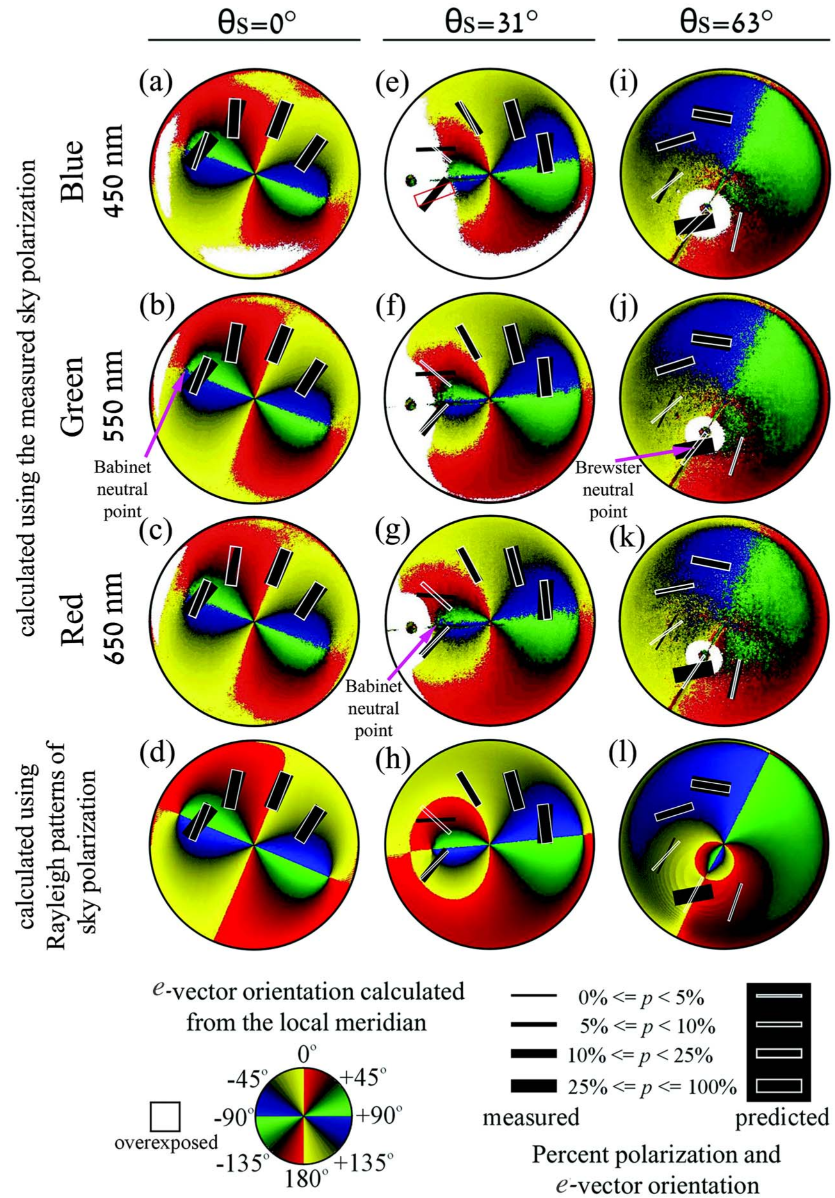

Fig. 3. (Color online) Predicted celestial *e*-vector orientation patterns viewed from water through Snell's window of a flat water surface at sun altitudes $\theta_S = 0°$, 31°, and 64°. Patterns are calculated from the Fresnel theory of refraction using measurements at (a), (e), (i) 450, (b), (f), (j) 550, and (c), (g), (k) 650 nm and (d), (h), (l) Rayleigh celestial patterns. Due to refraction of light, the center and the perimeter of the circular patterns are the zenith and the boundary of Snell's window, respectively, and the apparent sun altitudes are $\theta_S = 41.26°$, 49.86°, and 70.43°. Black bars and white rectangles represent the measured and predicted percent polarization and *e*-vector orientation at several detector positions (coinciding with the centers of the bars). The alignment of the bars and rectangles shows the orientation of polarization, while their width corresponds to their percent polarization range.

measured polarization values ($d_{\text{semiempirical}} - d_{\text{measured}}$ and $\alpha_{\text{semiempirical}} - \alpha_{\text{measured}}$) within Snell's window varied neither with sun altitude (Kruskal–Wallis, $H_{2,44} = 1.31$, $p > 0.5$ and $H_{2,44} = 0.53$, $p > 0.7$, Figs. 1 and 2) nor with the light hue (Kruskal–Wallis, $H_{2,44} = 2.67$, $p > 0.2$ and $H_{2,44} = 0.52$, $p > 0.9$, Fig. 3) for d and α, respectively. The Snell's window polarization parameters calculated with the single-scattering Rayleigh model and the Fresnel theory of refraction were compared with the corresponding measured values in the green spectral region (550 nm). No significant effect of the sun altitude on the degree of fit between the theoretical prediction and the measured polarization values ($d_{\text{Rayleigh}} - d_{\text{measured}}$ and $\alpha_{\text{Rayleigh}} - \alpha_{\text{measured}}$) was found (Kruskal–Wallis, $H_{2,15} = 2.24$, $p > 0.3$ and $H_{2,15} = 0.8$, $p > 0.9$, Fig. 3). Consequently, performing analyses on the pooled measurements from the different sun altitudes and wavelengths was possible.

The polarization patterns within Snell's window, calculated by using either the celestial Rayleigh pattern (d_{Rayleigh} and α_{Rayleigh}) or the measured celestial pattern ($d_{\text{semiempirical}}$ and $\alpha_{\text{semiempirical}}$), did not vary from each other (Wilcoxon, $n = 15$, $p > 0.6$ and $p > 0.3$ for d and α values, respectively, Fig. 2) through all examined sun altitudes and directions. Within Snell's window, *e*-vector orientations predicted by both the semiempirical calculations ($\alpha_{\text{semiempirical}}$) and the celestial Rayleigh pattern (α_{Rayleigh}) did not differ significantly (Wilcoxon, $n=44$ and 15, $p>0.17$) and were highly correlated [$R^2=0.96$ and 0.73, respectively, $p<0.001$, Figs. 4(c) and 4(d)] with the corresponding measured values (α_{measured}). Throughout all measurements, the values of $|\alpha_{\text{semiempirical}}-\alpha_{\text{measured}}|$ and $|\alpha_{\text{Rayleigh}}-\alpha_{\text{measured}}|$ were $12.43°\pm13.06°$ and $12.39°\pm15.54°$ (average ± SD), respectively. On the other hand, percent polarization predicted by both the semiempirical calculations ($d_{\text{semiempirical}}$) and the celestial Rayleigh pattern (d_{Rayleigh}) was found to differ significantly from the measured (d_{measured}) ones (Wilcoxon, $n=44$ and 15, $p<0.05$). They were both lower than the measured (d_{measured}) values [$d_{\text{semiempirical}}-d_{\text{measured}}=-9.86\%\pm9.37\%$ (Average ± SD), sign test, $n=44$, $p<0.05$, Fig. 3(a); $d_{\text{Rayleigh}}-d_{\text{measured}}=-8.75\%\pm10.65\%$, sign test, $n=15$, $p<0.001$, Fig. 4(b)], yet both were significantly correlated with d_{measured} [$R^2=0.69$ and 0.62, respectively, $p<0.001$ Figs. 4(a) and 4(b)].

Within Snell's window, d was found to be wavelength dependent and to fit four major wavelength dependency patterns [Fig. 5(a)]. These patterns were defined by the relationship between d at different wavelengths: type 1 ($d_{350}<d_{450}>d_{700}$, like a downward-opening parabola), type 2 ($d_{350}>d_{500}>d_{700}$, generally decreasing with wavelength), type 3 ($d_{350}>d_{500}<d_{700}$, like an upward-opening parabola), and type 4 ($d_{350}<d_{500}<d_{700}$, generally increasing with wavelength). When sun altitude ranged between 0° and 20°, d at both edges of the measured spectrum (UV and red parts) was minimal, while the maximal d was reached at the middle of the spectrum, ~450 nm [type 1, Fig. 5(b)]. At greater sun altitudes (20°–80°), d decreased with wavelength, attaining its maximum in the UV part of the spectrum [type 2, Fig. 5(b)]. This held for directions away from the sun (180° − ~90°). However, as the line of sight approached the bearing of the sun, d became maximal at both edges of the spectrum [type 3, Fig. 5(b)] or at long wavelengths [type 4, Fig. 5(b)].

To evaluate the spectral differences in polarization, we calculated several parameters: the range of percent polarization across the measured spectrum (maximum—

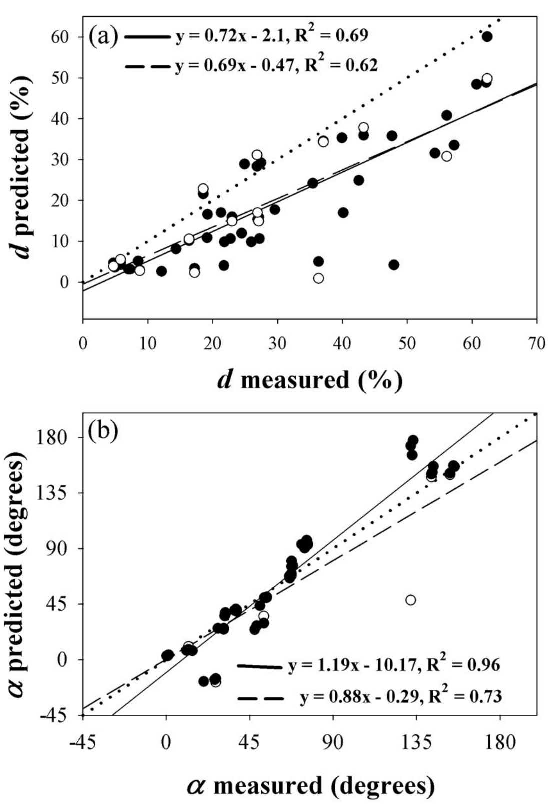

Fig. 4. Measured versus predicted (a) percent polarization and (b) *e*-vector orientation of skylight viewed from water through Snell's window. Solid lines, predicted polarization using measured celestial patterns at 450 and 650 nm (solid circles, $n=29$) and 550 nm (open circles, $n=15$); dashed lines, predicted polarization using the Rayleigh celestial patterns (compared only with the measured values at 550 nm); dotted lines, identity ($y=x$). In all cases, $p<0.001$. Polarization values within Snell's window, predicted in both manners, did not vary from each other (Wilcoxon, $n=15$, $p>0.6$ and $p>0.3$ for d and α values, respectively).

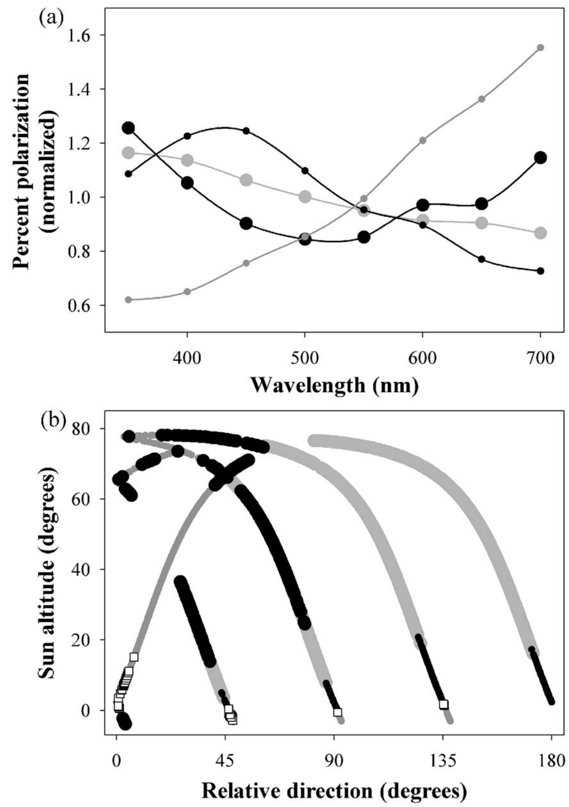

Fig. 5. Changes in percent polarization according to wavelength within Snell's window. (a) Gray and black circles represent individual measurements serving as examples of the four main "wavelength dependency patterns," classified as type 1 (small black circles), type 2 (large gray circles), type 3 (large black circles), and type 4 (small gray circles). Dependency types were defined by the relative relationships of the percent polarization values at given wavelengths; type 1 ($d_{350}<d_{450}>d_{700}$, similar to a downward-opening parabola), type 2 (decreasing with wavelength, $d_{350}>d_{500}>d_{700}$), type 3 ($d_{350}>d_{500}<d_{700}$, similar to an upward-opening parabola), and type 4 ($d_{350}<d_{500}<d_{700}$, increasing with wavelength). (b) Dependency types, appearing as circles, at different combinations of the sun's altitude and relative direction. Measurements that did not fit any of these dependency patterns were classified as type 0 and are depicted by open squares. Each point represents a single measurement [such as the ones presented in (a)]. Traces originate from measurements taken with the sensor fixed at one of five relative directions (0°, 45°, 90°, 135°, and 180° away from the sunrise meridian), while the sun changes altitude during the day's measurements.

minimum; Δd), the averaged percent polarization across this spectrum (d_{av}), and the maximal difference in the *e*-vector orientation across this spectral range ($\Delta\alpha$). All parameters were calculated based on measurements taken at eight distinct wavelengths between 350 and 700 nm and with a 50 nm interval. Both $\Delta d/d_{\mathrm{av}}$ [Fig. 6(a)] and $\Delta\alpha$ [Fig. 6(b)] increased with sun altitude. At low sun altitudes, the maximal $\Delta d/d_{\mathrm{av}}$ and $\Delta\alpha$ were achieved at a relative direction of 45° away from the sun and the minimal values were attained at a relative direction of 135° from the sun. However, as the sun altitude increased, the relative directions in which the maximal and minimal $\Delta d/d_{\mathrm{av}}$ occurred approached the sun and the antisun directions, respectively. Throughout all sun altitudes and relative directions, $\Delta d/d_{\mathrm{av}}$ and $\Delta\alpha$ ranged between 0.04 and 1.9 and 1° and 52°, respectively. In over 50% of the measurements, d was highest in the 350–400 nm range. Additionally, when $\Delta d/d_{\mathrm{av}}$ assumed high values, the highest d was found at both ends of the spectrum, namely at 350–400 nm and 700 nm [Fig. 6(c)].

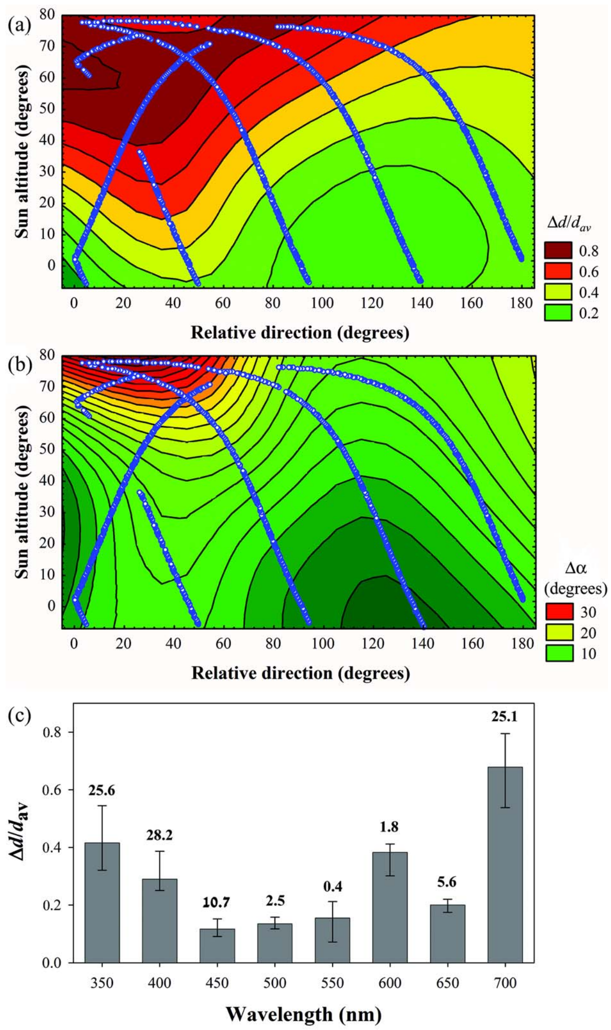

Fig. 6. (Color online) Distribution of differences between wavelengths in (a) percent polarization ($\Delta d/d_{\mathrm{av}}$) and (b) *e*-vector orientation ($\Delta\alpha$) as a function of the sun altitude and relative direction. Δd is defined as the maximal difference in the percent polarization between any examined wavelengths, and d_{av} as the percent polarization averaged over the eight examined wavelengths (350–700 nm, with a 50 nm interval). $\Delta\alpha$ is defined as the maximal difference in the *e*-vector orientation between wavelengths. In (a) and (b), dots represent individual measurements taken at a certain combination of sun altitude and relative direction, and surfaces stand for an extrapolation (distance-weighted least squares) calculated from the measurements. Sun altitude is measured off the horizon, while the relative direction corresponds to the horizontal angular distance between the directions of the line of sight and the sun. (c) Median $\Delta d/d_{\mathrm{av}}$ (with the first and third quartiles) as a function of the wavelength at which the maximal percent polarization was attained. The proportion of measurements in which the maximal percent polarization was attained at the indicated wavelength is provided above each bar.

4. DISCUSSION

Both the semiempirical and Rayleigh calculations of predicted percent polarization d and *e*-vector orientation α of skylight transmitted through a flat water surface were comparable with and correlated with the underwater measured values. Therefore the change in the state of polarization of skylight transmitted through the water surface can be well described by the Fresnel theory of refraction. These results show that the celestial polarization pattern is indeed available to shallow living marine animals, despite the effects of refraction at the undulating water surface. Although correlated, the measured values of d were significantly higher than those predicted by using either the measured or the Rayleigh skylight (Fig. 4). These differences can be attributed to technical restrictions or to environmental/optical factors not considered in the calculations:

(i) The bandwidths and spectral response of the underwater point-source polarimeter and the aerial full-sky imaging polarimeter were different.

(ii) The celestial polarization patterns used for the semiempirical prediction were measured in Tunisia in 1999, while the underwater measurements occurred in Israel in 2003, during which the sky polarization patterns were unknown. However, the close resemblance of the semiempirical and Rayleigh predictions suggests that this difference was not a significant factor.

(iii) In all presented calculations, the absorbing and scattering effects of the 2 m seawater layer above the detector were neglected.

(iv) The water surface was assumed to be flat (without water ripples) in all calculations, while during the underwater measurements the sea surface was inevitably undulated.

The first two limitations [(i) and (ii)] apply only to the semiempirical prediction, while the last two [(iii) and (iv)] apply to both manners of prediction. Therefore we conclude that the environmental/optical factors are primarily responsible for the dissimilarities between the predicted and measured polarization. These are the effects of the optical properties of water, the light's path length within the water, and the surface waves. Consequently, we anticipate that the correlation between the measured and predicted polarization within Snell's window will be highest right under a calm water surface and will decrease with depth. This decrease will grow faster with water turbidity. Eventually, the Snell's window polarization pattern is predicted to become similar to that of the bulk underwater polarization at depths of 10–15 m, depending on water turbidity.[11] Indeed, measuring at a depth of 15 m, Cronin and Shashar[12] found small (if any) differences between the two polarization patterns. Moreover, colored dissolved organic matter and solutes change the spectral distribution of light. Generally, the percent polarization decreases with an increase in the share of scattering in the total light attenuation,[44,45] that is, with a decrease of the ratio a/b, where a and b are the volume absorption and scattering coefficients, respectively. Thus enhanced Rayleigh scattering near absorption edges of water or solutes is expected to diminish the percent polarization and thus to change its spectral distribution. However, scattering by particles of the size order of Mie scattering (1–3 μm) was demonstrated to increase the percent polarization.[12,46] Both cases are expected to diminish the apparent celestial polarization pattern. However, the exact effect of colored solutes, common in shallow coastal waters, on the distribution of polarized light and its availability to animal vision requires further study.

The Rayleigh model and the semiempirical approach yielded similar polarization patterns within Snell's window. This is due to the similarity between the measured and the Rayleigh skylight (Wilcoxon, $n=15$, $p>0.3$ for both α and d). Indeed, Suhai and Horváth[47] showed that the single-scattering Rayleigh theory well describes the e-vector orientation of skylight in most regions of a clear sky. However, they also reported on well-defined differences between the Rayleigh prediction and the measured sky polarization, especially around the sun and antisun, where the neutral points of skylight polarization occur. Our findings of considerable differences between the measured and predicted polarization parameters near the Babinet neutral point [Figs. 1(f), 2(a)–2(c), and 2(e)–2(g)], near the Brewster neutral point [Figs. 1(r) and 2(i)–2(k)], and in the vicinity of the overexposed sky regions [Figs. 3(e)–3(g)] are in accordance with the report of Suhai and Horváth.[47] Neutral points are the unique sites in the sky dome from which unpolarized skylight (with degree of linear polarization $d=0$) is radiated. They are named after their first observers. The Babinet neutral point (discovered by the French meteorologist Jacques Babinet in 1840) is placed along the solar meridian at about 25°–30° above the sun. The Brewster neutral point (discovered by the Scottish physicist David Brewster in 1842) is placed along the solar meridian at about 25°–30° below the sun. An overview about all four neutral points of atmospheric polarization has been given by Gal *et al.*[40] and Horváth *et al.*[48] Passing a neutral point along a meridian, the e-vector alignment suffers a turn of 90° because the neutral points are placed at the border of the celestial regions with positive (perpendicular to the plane of scattering, coded by bright blue and green colors in Fig. 2) and negative (parallel to the plane of scattering, coded by bright yellow and red colors in Fig. 2) skylight polarization.

Within Snell's window, the percent polarization as well as the e-vector orientation is wavelength dependent (for polarization dependence on wavelength outside Snell's window, see Cronin and Shashar[12] and Ivanoff and Waterman[46]). Rather than being constant, the mode of this dependency varies with the position of the sun, and thus it changes throughout the day. In most sunlit periods of the day (85% of the measurements), and at the majority of relative directions and sun altitudes, the percent polarization assumed its maximal value at the UV and red (700 nm) ends of the measured spectrum.

Many biological visual tasks require the determination of the natural polarization pattern in the sky (within Snell's window) or the discrimination of background polarization from polarization arriving from an object. In such cases, improved sensitivity may be achieved if the animal's polarization sensitivity is tuned to spectral regions where high polarization occurs. In cases where the differences in polarization between wavelengths were large, high percent polarization was found at the short (350–400 nm) or long (700 nm) ends of the measured spectrum [Fig. 6(c)]. No specific wavelength sensitivity is advantageous for perception of skylight polarization under clear skies. However, under cloudy skies, detection of skylight polarization in the UV maximizes the usefulness of the skylight polarization pattern as a cue for orientation and navigation.[16] UV-polarization-based navigation is well documented in insects.[6] Since the polarization within Snell's window resembles the skylight polarization, the advantage of using the UV component of light is expected to hold also for the light in a shallow marine environment. Indeed, it was suggested that salmonids possessing UV polarization sensitivity[29] orient and even navigate by using the polarization pattern within Snell's window.[7,15] Planktivorous fishes also, on occasion, use polarization sensitivity for finding transparent food items.[25] The polarization of light reflected from the body of a prey or transmitted through it differs from that of the skylight polarization within Snell's window.[16] A polarization-sensitive predator could therefore perceive the camouflaging prey against the refraction–polarization pattern of skylight. Lythgoe[1] suggested an additional behavioral adaptation for enhancing the conspicuousness of transparent objects by examining the margins of Snell's window. Planktivorous fishes possess enhanced visual acuity and forage at the margins of Snell's window.[49,50] In shallow waters, Snell's window margins separate between two polarization patterns, one within the window and the other outside it.[5] These two patterns differ in their origin as well as in their characteristics. Due to surface waves, Snell's window margins move continuously. Searching for prey at elevations corresponding to these margins can be expected to highlight the prey against this everchanging polarization background. In other words, to a polarization-sensitive viewer, foraging at Snell's window margins, the prey may flicker and hence be easy to detect. If indeed polarization vision is used (during daytime) for plankton detection within or at the edge of Snell's window, one may predict that UV- or red-sensitive photoreceptors are important for such a task.[22,51]

At low sun altitudes, the maximal percent polarization is attained at a wavelength of about 450 nm. Hence we suggest that, for tasks performed mainly near dawn and dusk (low sun altitudes), polarization sensitivity will be centered in the blue spectral region, where a high light intensity penetrates the water.[52–54] The wavelength dependency of the polarization characteristics within Snell's window may have participated in spectrally tuning the photoreceptors in polarization-sensitive marine animals. However, critical experimental examination of this topic is desired.

ACKNOWLEDGMENTS

We thank R. Goldshmid, S. Einbinder, and Y. Belmaker for underwater and technical help; A. Rivlin for writing LabView applications for polarization calculations; I. Lerer, M. Ohavia, and E. Sarfati for fabricating the detector's anchoring and rotating apparatuses; R. Holzman and two anonymous reviewers for statistical advice and helpful comments; and C. Erlick, M. Kiflawi, and T. W. Cronin for enlightening discussions. This research was supported by Binational Science Foundation (BSF) grant 1999040, Israel Science Foundation (ISF) grant 550/03, the Ring Foundation, and an István Széchenyi research fellowship (the latter received by G. Horváth from the Hungarian Ministry of Education).

Address correspondence to Nadav Shashar, nadavs@huji.ac.il. Gábor Horváth's e-mail address is gh@arago.elte.hu.

REFERENCES

1. J. N. Lythgoe, *The Ecology of Vision* (Oxford U. Press, 1979).
2. T. H. Waterman, "Polarization sensitivity," in *Comparative Physiology and Evolution of Vision in Invertebrates. B: Invertebrate Visual Centers and Behavior I*, H. Autrum, ed. (Springer-Verlag, 1981), pp. 281–469.
3. W. G. Egan, *Photometry and Polarization in Remote Sensing* (Elsevier, 1985).
4. A. Ivanoff and T. H. Waterman, "Elliptical polarization of submarine illumination," J. Mar. Res. **16**, 255–282 (1958).
5. T. H. Waterman, "Polarization patterns in submarine illumination," Science **120**, 927–932 (1954).
6. R. Wehner, "Polarization vision—a uniform sensory capacity?" J. Exp. Biol. **204**, 2589–2596 (2001).
7. G. Horváth and D. Varjú, "Underwater refraction–polarization patterns of skylight perceived by aquatic animals through Snell's window of the flat water surface," Vision Res. **35**, 1651–1666 (1995).
8. H. Schenck, "On the focusing of sunlight by ocean waves," J. Opt. Soc. Am. **47**, 653–657 (1957).
9. R. L. Snyder and J. Dera, "Wave-induced light-field fluctuations in the sea," J. Opt. Soc. Am. **60**, 1072–1079 (1970).
10. M. Stramska and T. D. Dickey, "Short-term variability of the underwater light field in the oligotrophic ocean in response to surface waves and clouds," Deep-Sea Res., Part I **45**, 1393–1410 (1998).
11. N. Shashar, S. Sabbah, and T. W. Cronin, "Transmission of linearly polarized light in sea water: implications for polarization signaling," J. Exp. Biol. **207**, 3619–3628 (2004).
12. T. W. Cronin and N. Shashar, "The linearly polarized light field in clear, tropical, marine waters: spatial and temporal variation of light intensity, degree of polarization and e-vector angle," J. Exp. Biol. **204**, 2461–2467 (2001).
13. V. A. Timofeyeva, "The degree of polarization of light in turbid media," Izv. Acad. Sci. USSR Atmos. Oceanic Phys. **6**, 513–522 (1970).
14. V. A. Timofeyeva, "Plane of vibrations of polarized light in turbid media," Izv. Acad. Sci. USSR Atmos. Oceanic Phys. **5**, 1049–1057 (1969).
15. I. Novales Flamarique and C. W. Hawryshyn, "Is the use of underwater polarized light by fish restricted to crepuscular time periods?" Vision Res. **37**, 975–989 (1997).
16. G. Horváth and D. Varjú, *Polarized Light in Animal Vision: Polarization Patterns in Nature* (Springer-Verlag, 2003).
17. C. Groot, "On the orientation of young sockeye salmon (*Oncorhynchus nerka*) during their seaward migration out of lakes," Behaviour (Suppl.) **14**, 1–198 (1965).
18. T. H. Waterman and R. B. Forward, "Field evidence for polarized light sensitivity in the fish *Zenarchopterus*," Nature **228**, 85–87 (1970).
19. R. B. Forward, K. W. Horch, and T. H. Waterman, "Visual orientation at the water surface by the teleost *Zenarchopterus*," Biol. Bull. **143**, 112–126 (1972).
20. R. B. Forward and T. H. Waterman, "Evidence for e-vector and light intensity pattern discrimination by the teleost *Demogenys*," J. Comp. Physiol. **87**, 189–202 (1973).
21. H. Kleerekoper, J. H. Matis, A. M. Timms, and P. Gensler, "Locomotor response of the goldfish to polarized light and its e-vector," J. Comp. Physiol. **86**, 27–36 (1973).
22. C. W. Hawryshyn, M. G. Arnold, D. Bowering, and R. L. Cole, "Spatial orientation of rainbow trout to plane-polarized light: the ontogeny of e-vector discrimination and spectral characteristics," J. Comp. Physiol., A **166**, 565–574 (1990).
23. C. W. Hawryshyn, "Polarization vision in fish," Am. Sci. **80**, 479–491 (1992).
24. R. Schwind, "*Daphnia pulex* swims towards the most strongly polarized light—a response that leads to 'shore flight'," J. Exp. Biol. **202**, 3631–3635 (1999).
25. I. Novales Flamarique and H. I. Browman, "Foraging and prey-search behavior of small juvenile rainbow trout (*Oncorhynchus mykiss*) under polarized light," J. Exp. Biol. **204**, 2415–2422 (2001).
26. N. G. Jerlov, "Significant relationships between optical properties of the sea," in *Optical Aspects of Oceanography*, N. G. Jerlov and E. S. Nielsen, eds. (Academic, 1974), pp. 77–94.
27. N. J. Jerlov, *Optical Oceanography*, Vol. 5 of Elsevier Oceanography Series (Elsevier, 1968).
28. C. W. Hawryshyn and W. N. McFarland, "Cone photoreceptor mechanisms and the detection of polarized light in fish," J. Comp. Physiol., A **160**, 459–465 (1987).
29. D. C. Parkyn and C. W. Hawryshyn, "Polarized light sensitivity in rainbow trout (*Oncorhynchus mykiss*): characterization from multiunit ganglion cell responses in the optic nerve fibers," J. Comp. Physiol., A **172**, 493–500 (1993).
30. G. S. Loesy, T. W. Cronin, T. H. Goldsmith, D. Hyde, N. J. Marshall, and W. N. McFarland, "The UV visual world of fishes: a review," J. Fish Biol. **54**, 921–943 (1999).
31. S. M. Goddard and R. B. Forward, "The use of celestial cues in the offshore escape response of the shrimp, *Palaemonetes vulgaris*," Mar. Behav. Physiol. **16**, 11–18 (1989).
32. S. M. Goddard and R. B. Forward, "The decay and learning of a *y* axis orientation behavior: the offshore escape response of the shrimp *Palaemonetes vulgaris* (Say)," J. Exp. Mar. Biol. Ecol. **142**, 137–150 (1990).
33. S. M. Goddard and R. B. Forward, "The role of the underwater polarized light pattern, in sun compass navigation of the grass shrimp, *Palaemonetes vulgaris*," J. Comp. Physiol., A **169**, 479–491 (1991).
34. D. A. Ritz, "Polarized-light responses in the shrimp *Palaemonetes vulgaris* (Say)," J. Exp. Mar. Biol. Ecol. **154**, 245–250 (1991).
35. N. Shashar, R. T. Hanlon, and A. D. Petz, "Polarization vision helps detect transparent prey," Nature **393**, 222–223 (1998).
36. E. J. Denton and J. A. C. Nicol, "Polarization of light reflected from the silvery exterior of the bleak *Alburnus alburnus*," J. Mar. Biol. Assoc. U.K. **45**, 705–709 (1965).
37. N. Shashar, R. Hagen, J. G. Boal, and R. T. Hanlon, "Cuttlefish use polarization sensitivity in predation on silvery fish," Vision Res. **40**, 71–75 (2000).

38. L. B. Wolff and A. G. Andreou, "Polarization camera sensors," Image Vis. Comput. **13**, 497–509 (1995).
39. I. Pomozi, G. Horváth, and R. Wehner, "How the clear-sky angle of polarization pattern continues underneath clouds: full-sky measurements and implications for animal orientation," J. Exp. Biol. **204**, 2933–2942 (2001).
40. J. Gál, G. Horváth, V. B. Meyer-Rochow, and R. Wehner, "Polarization patterns of the summer sky and its neutral points measured by full-sky imaging polarimetry in Finnish Lapland north of the Arctic Circle," Proc. R. Soc. London, Ser. A **457**, 1385–1399 (2001).
41. A. Barta and G. Horváth, "Underwater binocular imaging of aerial objects versus the position of eyes relative to the flat water surface," J. Opt. Soc. Am. A **20**, 2370–2377 (2003).
42. K. L. Coulson, *Polarization and Intensity of Light in the Atmosphere* (Deepak, 1988).
43. E. Collett, *Polarized Light—Fundamentals and Applications* (Marcel Dekker, 1994).
44. A. Ivanoff, "Polarization measurements in the sea," in *Optical Aspects of Oceanography*, N. G. Jerlov and E. S. Nielsen, eds. (Academic, 1974), pp. 151–175.
45. V. A. Timofeyeva, "Optics of turbid waters (results of laboratory studies)," in *Optical Aspects of Oceanography*, N. G. Jerlov and E. S. Nielsen, eds. (Academic, 1974), pp. 177–219.
46. A. Ivanoff and T. H. Waterman, "Factors, mainly depth and wavelength, affecting the degree of underwater light polarization," J. Mar. Res. **16**, 283–307 (1958).
47. B. Suhai and G. Horváth, "How well does the Rayleigh model describe the E-vector distribution of skylight in clear and cloudy conditions? A full-sky polarimetric study," J. Opt. Soc. Am. A **21**, 1669–1676 (2004).
48. G. Horváth, B. Bernath, B. Suhai, A. Barta, and R. Wehner, "First observation of the fourth neutral point in the atmosphere," J. Opt. Soc. Am. A **19**, 2085–2099 (2002).
49. O. Munk, "On the occurrence and significance of horizontal band-shaped retinal areas in teleosts," Vidensk. Medd. Dan. Naturhist. Foren. **133**, 85–120 (1970).
50. J. Janssen, "Searching for zooplankton just outside Snell's window," Limnol. Oceanogr. **26**, 1168–1171 (1981).
51. C. W. Hawryshyn, H. D. Moyer, W. D. Allison, T. J. Haimberger, and W. N. McFarland, "Multidimensional polarization sensitivity in damselfishes," J. Comp. Physiol., A **189**, 213–220 (2003).
52. W. N. McFarland, "Light in the sea—correlations with behaviors of fishes and invertebrates," Am. Zool. **26**, 389–401 (1986).
53. W. N. McFarland, "The visual world of coral reef fishes," in *The Ecology of Fishes on Coral Reefs* (Academic, 1991), pp. 16–37.
54. W. N. McFarland, C. M. Wahl, T. H. Suchanek, and F. A. McAlary, "The behavior of animals around twilight with emphasis on coral reef communities," in *Adaptive Mechanisms in Ecology of Vision*, S. N. Archer, ed. (Academic, 1999), pp. 583–628.